Modeling of Amorphous Polyaniline Emeraldine Base

Manel Canales,*,† David Curcó,‡ and Carlos Alemán*,§,||

Departament de Física i Enginyeria Nuclear, Facultat d'Informàtica, Universitat Politècnica de Catalunya, Jordi Girona 1-3, Barcelona E-08034, Spain, Departament d'Enginyeria Química, Facultat de Química, Universitat de Barcelona, Martí i Franquès 1, Barcelona E-08028, Spain, Departament d'Enginyeria Química, ETS d'Enginyeria Industrial de Barcelona, Universitat Politècnica de Catalunya, Diagonal 647, 08028 Barcelona, Spain, and Center for Research in Nano-Engineering, Universitat Politècnica de Catalunya, Campus Sud, Edifici C′, C/Pasqual i Vila s/n, 08028 Barcelona, Spain

Received: June 8, 2010

Amorphous polyaniline emeraldine base has been investigated using atomistic classical molecular dynamics simulations. Initially, different sets of force-field parameters, which differ in the atomic charges and/or the van der Waals parameters, were tested. The experimental density of polyaniline was satisfactorily reproduced using the following combination: (i) equilibrium bond lengths, equilibrium bond angles, and electrostatic charges derived from quantum mechanical calculations and (ii) van der Waals parameters extrapolated from GROMOS for all atoms with the exception of the CH pseudoparticles of the phenyl ring, which were taken from an anisotropic united atom potential. Next, this force field was used to investigate the structure of the polymer in the amorphous state, the trajectories performed for this purpose allowing accumulation of 750 ns. Analyses of the energies evidence that the interactions between one repeating unit containing an amine nitrogen atom and another unit with an imine nitrogen are favored with respect to those between two identical repeating units. This conclusion is also supported by quantum mechanical and quantum mechanical/molecular mechanics calculations. On the other hand, the partial radial distribution functions indicate that this material only exhibits short-range intramolecular correlation, which is in excellent agreement with experimental evidence.

Introduction

In recent years a large number of quantum mechanical studies have been devoted to examine the structural and electronic properties of conducting oligomers and polymers at the molecular level, i.e., polythiophene (PPy), polypyrrole (PTh), polyaniline (PAni), and their derivatives.[1,2] Among all these conducting polymers, PAni has experimented a continued growing in its technological use, which should be attributed to its excellent properties: high chemical and environmental stabilities, remarkable electrical conductivity in the doped state, easy processability, and low cost. To date, PAni has found widespread applications ranging from anticorrosion coatings to chemical sensors, electrodes, capacitors, and batteries. This led us to apply quantum mechanical methodologies to rationalize the electronic structure of such material at the molecular level when it is in the undoped and the doped states.[2f,g]

In practical polymer science, however, there is a number of interesting problems related to PAni that refer to the organization of the molecular chains, which consist of C_6H_4-N repeating units, in condensed phases. Many of these problems are related to the three-dimensional disposition of the molecular chain in solution. For example, the nonconducting form of PAni is difficult to disperse, even in commonly used organic solvents like *n*-methyl-2-pyrrolidinone.[3] Furthermore, short-term storage of nonconducting PAni gives rise to gelation, which has been attributed to the formation of interchain hydrogen bonds,[4] and the chain conformation in solution has been suggested to have a large impact on the conductivity of the polymer thin film.[5] Some of these problems were recently addressed in a comprehensive molecular dynamics (MD) study using both atomistic molecular mechanics and coarse-grained potentials.[6] In such work, Hua and co-workers examined single chain and aggregation properties of nonconducting PAni in solution. In spite of this, the microscopic knowledge of the structural properties of PAni in the solid state are practically negligible.[7,8] Specifically, in a recent work Ostwal and co-workers investigated the diffusion and sorption of water in doped PAni.[7] More recently, in a very simple study Bhadra and Khastgir examined the glass−rubber transition temperature by considering one polymer chain within a simulation box and applying periodic boundary conditions.[8] Given that in many of its technological applications PAni is used in the solid state, e.g., as a film, it appears crucial to gain a comprehensive understanding into the characteristics of this conducting polymer in the solid state.

In this work we investigate the molecular organization of the most frequent form of nonconducting PAni, denoted emeraldine base (EB) form, using atomistic MD simulations. PAni-EB is obtained by treating the conducting emeraldine salt (ES) form with a base (Scheme 1) and involves both amine and imine nitrogen atoms; i.e., half of the nitrogen atoms are oxidized. Accordingly, the relative distribution of the repeating units containing amine and imine nitrogen atoms, hereafter referred to as AM and IM units, respectively, has been examined from both intramolecular and intermolecular points of view. For this purpose, a number of systems, which differ in the distribution of the AM and IM units, has been considered for simulation.

* To whom correspondence should be addressed. E-mail: manel.canales@upc.edu (M.C.); carlos.aleman@upc.edu (C.A.).
† Facultat d'Informàtica, Universitat Politècnica de Catalunya.
‡ Universitat de Barcelona.
§ ETS d'Enginyeria Industrial de Barcelona, Universitat Politècnica de Catalunya.
|| Center for Research in Nano-Engineering, Universitat Politècnica de Catalunya.

10.1021/jp1052584
Published on Web 07/12/2010

SCHEME 1

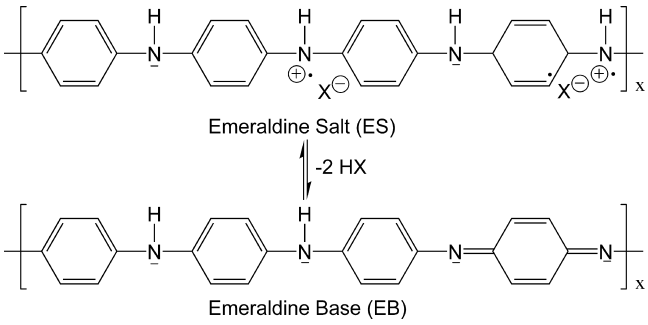

This article is organized as follows. In the next section we present both the molecular models studied in this work and the generation of reliable starting atomistic microstructures for such models using a procedure based on a random search of energy minima. After this, force-field parameters able to describe PAni-EB are properly selected. Specifically, eight different sets of nonbonding parameters have been checked, even though only a few of them were able to reproduce satisfactorily the experimental density of PAni-EB using MD. Next, we use three different theoretical methodologies (MD, quantum mechanics, and quantum mechanics/molecular mechanics) to examine the stability of the different molecular models proposed for PAni-EB. After this, the snapshots recorded during MD trajectories are used to examine the structural properties. Finally, the conclusions are outlined in the last section.

Molecular Models and Generation of Starting Microstructures

Four different molecular models, each one consisting of 100 a.m. and 100 IM repeating units distributed in four chains of identical molecular weight, have been considered for PAni-EB. In the first one (model **I**) each chain involves 25 a.m. units attached to 25 IM units following a block structure, i.e., $AM_{25}-IM_{25}$. The four chains of the second model (model **II**) are formed by an alternative distribution of AM and IM units, i.e. $(AM-IM)_{25}$. In model **III** each chain presents 25 a.m. and 25 IM units randomly distributed. Finally, model **IV** corresponds to a system formed by two $(AM)_{50}$ chains and two $(IM)_{50}$ chains. In all cases chains were blocked with a phenyl ring at the two ends. It should be noted that model **I** has been only used for the choice of the force-field parameters (see next section) while models **II**, **III**, and **IV**, which describe the situations with the largest differences, have been examined to investigate the microstructure of PAni-EB.

Scheme 2 shows the labels used to identify the atom types of the AM and IM repeating units, which will be essential for the parametrization process (see next section). As can be seen, the atom types are identical for all the AM units, independent of their neighbors, while two different sets of atom types have been defined for the IM units: one for those covalently linked to AM units and the other for the rest. It is worth noting that, for computational efficiency reasons, the C_6H_4 rings of both AM and IM units were represented using a pseudoatom model for the C−H groups (united atom approximation).

Microstructures of the four models under study, which have been used as starting points of MD simulations (see below), were produced using the SuSi (Structure Simulation) computer strategy.[9] This method was recently developed to generate and relax atomistic microstructures of amorphous polycyclic materials. The method is an extension of a procedure previously reported for study of linear amorphous polymers,[10,11] consisting of a generation algorithm that eliminates the torsion strain and a simple Monte Carlo Metropolis method to relax the generated structures. Specifically, 10 microstructures, each one consisting of 4 packed chains, were generated for each of the 4 models considering the density experimentally determined for PAni-EB ($\rho = 1.245$ g/cm^3).[12]

Force-Field Parametrization and Simulation Conditions

Before examination of the relative stabilities and structural characteristics of the models considered for PAni-EB, a reliable set of force-field parameters for MD was required. Equilibrium bond lengths and bond angles (l_0 and θ_0, respectively) were extrapolated from a recent quantum mechanical study.[2f] Table 1 lists the values of l_0 and θ_0 for the bond lengths and bond angles, respectively, involving the different atom types of the AM and IM units. These parameters were taken from the molecular geometries of PAni-EB oligomers optimized using the BH and H functional combined with the 6-31G(d) basis set.[2f] Similarly, torsional parameters were derived from previously reported quantum results.[2f] Regarding the van der Waals and electrostatic interactions, which were represented using a Lennard-Jones and a Coulombic potential, respectively, the following sets of nonbonding parameters were tested:

(a) Force field 1 (**FF1**). Van der Waals parameters were taken from the GROMOS 53A6 parametrization,[13] in which Lennard-Jones pair potential parameters are computed as the geometric mean of the component atom values. Electrostatic parameters were obtained by fitting the rigorously defined quantum mechanical molecular electrostatic potential, which was computed at the HF/6-31G(d) level,[14] to the Coulombic electrostatic potential through a Levenberg−Marquardt nonlinear optimization procedure.

(b) Force fields 2 and 3 (**FF2** and **FF3**). These force fields only differ from **FF1** in the electrostatic parameters, which were obtained by imposing some restrictions in the fitting procedure, i.e., absence of charge in some atoms of the phenyl rings (**FF2**) and excess of negative charge at the nitrogen atoms to favor the formation of N−H···N hydrogen bonds (**FF3**).

(c) Force field 4 (**FF4**). The van der Waals parameters of the nitrogen atoms were derived by fitting the Buckingham potentials involving such atom types and derived using the MM2 parameters of Allinger and co-workers[15] to a Lennard-Jones potential. The rest of the parameters, including the electrostatic ones, are identical to those of **FF1**.

(d) Force fields 5, 6, and 7 (**FF5**, **FF6**, and **FF7**). These force fields only differ from **FF4** in the van der Waals parameters of the CH pseudoatoms (atom types CB, CD, and CF), which were taken from the force fields developed by Siepmann and co-workers[16] (**FF5**), Errington and Panagiotopoulus[17] (**FF6**), and Mackie and co-workers[18] (**FF7**).

SCHEME 2

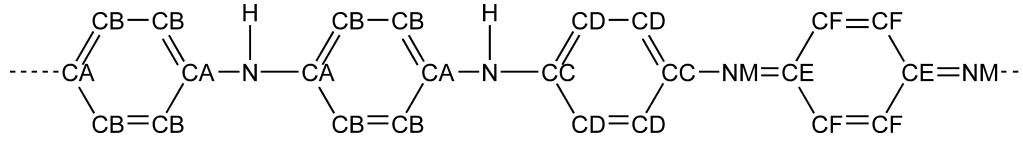

TABLE 1: Equilibrium Bond Lengths and Bond Angles (l_0 and θ_0, Respectively) Force-Field Parameters for PAni-EB

AM unit		IM unit		AM unit		IM unit	
bond[a]	l_0 (Å)	bond[a]	l_0 (Å)	angle[a]	θ_0 (°)	angle[a]	θ_0 (°)
CA−CB	1.387	CC−CD	1.391	CA−CB−CB	121.1	CC−CD−CD	120.8
CA−N	1.380	CC−NM	1.376	CA−N−CA	127.3	CC−NM−CE	123.1
CB−CB	1.375	CD−CD	1.373	CA−N−H	116.1	CD−CC−CD	118.3
N−H	1.003	CE−CF	1.450	CB−CA−CB	117.7	CD−CC−NM	120.7
		CE−NM	1.278	CB−CA−N	121.1	CE−CF−CF	121.7
		CF−CF	1.332			CF−CE−CF	116.7
						CF−CE−NM	121.6

[a] Atom types are indicated in Scheme 2.

TABLE 2: Electrostatic Parameters (in Units of Electron) for the Different Force Fields Used To Describe PAni-EB

atom type[a]	FF1[b]	FF2	FF3
N	−0.698	−0.398	−0.798
H	0.376	0.276	0.476
CA	0.361	0.061	0.461
CB	−0.100	0.000	−0.150
NM	−0.656	−0.356	−0.756
CC	0.481	0.155	0.631
CD	−0.105	0.000	−0.130
CE	0.551	0.201	0.601
CF	−0.083	0.000	−0.108

[a] Atoms types are indicated in Scheme 2. [b] Electrostatic parameters for **FF4**, **FF5**, **FF6**, **FF7**, and **FF8** are identical to those of **FF1**.

(e) Force field (**FF8**). This force field is identical to **FF1**, with the exception of the van der Waals parameters of the CH pseudoatoms, which were transferred from the anisotropic united atom potential developed by Mackie and co-workers.[18]

The electrostatic and van der Waals parameters of the eight force fields under consideration are listed in Tables 2 and 3, respectively. In order to ascertain the reliability of each force field, *NPT* (temperature 300 K and 1 atm of pressure) MD simulations were performed using as a starting point the microstructures generated for model **I**. MD simulations were performed using the GROMACS 4.2. program,[19] an integration step of 1 fs being selected. Atom pair distance cutoffs were applied at 10.0 Å to compute the van der Waals interactions. Electrostatic interactions were extensively computed by means of Ewald summations. The real space term was defined by the van der Waals cutoff, while the reciprocal space was computed by interpolation into an infinite grid of points (Particle Mesh Ewald) with maximum space grid points being 1.2 Å.[20] Before the production MD trajectory with each force field was run, the starting microstructure was equilibrated using the following strategy: 1×10^4 steps of energy minimization were performed in order to relax conformational and structural tensions. Next, 1.0 ns of *NPT*-MD at 300 K and 1 atm was used to equilibrate the molecular chains in the simulation box. Both temperature and pressure were controlled by the weak coupling method of the Berendsen thermobarostat,[21] using a time constant for the heat bath coupling and a pressure relaxation time of 1 ps. The coordinates of all the production runs were saved every 1000 steps (1 ps intervals). The *NPT*-MD production runs using the 8 force fields were 10 ns long.

Table 4 lists the averaged density, as well as its root-mean-square deviation (rmsd), derived from the eight tested force fields. As can be seen, the force field affects dramatically the density, the influence of the van der Waals parameters being particularly relevant. Thus, modification of the electrostratic parameters, which occurs in **FF1**, **FF2**, and **FF3**, produces a variation in the density that ranges from 0.978 to 1.031 g/cm^3, while **FF1** and **FF8** that only differ in the van der Waals parameters of the CH pseudoatoms provided densities of 1.009 and 1.289 g/cm^3, respectively. It is worth noting that the densities calculated using **FF7** and **FF8** (ρ= 1.271 and 1.289 g/cm^3) are the closest to the experimental value (ρ = 1.245 g/cm^3),[12] which is overestimated by only 2.1% and 3.5%, respectively. On the other hand, inspection of the low rmsd values displayed in Table 4 indicates that in all cases the evolution of density remains stable during the whole production trajectory. This is also illustrated in Figure 1, which shows the temporal evolution of the density during the trajectories performed using **FF1** and **FF8**. According to the results displayed in Table 4, the force field selected for the description of PAni-EB was **FF8**, only being used for the simulations presented in the next sections. The preference toward **FF8** against **FF7** was based on the fact that in the former all the van der Waals parameters with exception of those for the CH pseudoatom were directly taken from the GROMOS force field,[13] while in the latter the MM2 parameters[15] required a transformation.

TABLE 3: Van der Waals (σ and ε; in Å and kcal/mol, Respectively) Parameters for the Different Force Fields Used To Describe PAni-EB

	N[a]		C[b]		CH[c]		H[d]	
	σ	ε	σ	ε	σ	ε	σ	ε
FF1[e]	3.1365	0.1529	3.5812	0.0663	3.7412	0.1201	0.0000	0.0000
FF4	3.2025	0.0650	3.5812	0.0663	3.7412	0.1201	0.0000	0.0000
FF5	3.2025	0.0650	3.5812	0.0663	3.6950	0.1003	0.0000	0.0000
FF6	3.2025	0.0650	3.5812	0.0663	3.6950	0.1472	0.0000	0.0000
FF7	3.2025	0.0650	3.5812	0.0663	3.2464	0.1777	0.0000	0.0000
FF8	3.1365	0.1529	3.5812	0.0663	3.2464	0.1777	0.0000	0.0000

[a] N refers to atom types N and NM (Scheme 2). [b] C refers to atom types CA, CC, and CE (Scheme 2). [c] CH refers to atom types CB, CD, and CF (Scheme 2). [d] H refers to atom type H (Scheme 2). [e] Van der Waals parameters for **FF2** and **FF3** are identical to those of **FF1**.

TABLE 4: Density (ρ) Obtained for Model I Using the Eight Force Fields Tested in This Work[a]

	FF1	FF2	FF3	FF4	FF5	FF6	FF7	FF8
ρ (g/cm^3)	1.009	0.978	1.031	1.034	1.011	1.081	1.271	1.289
rmsd × 10^{-3} (g/cm^3)	4.4	4.1	4.2	4.0	4.3	3.7	4.7	4.3

[a] The rmsd of the density along the 10 ns MD trajectory is also displayed.

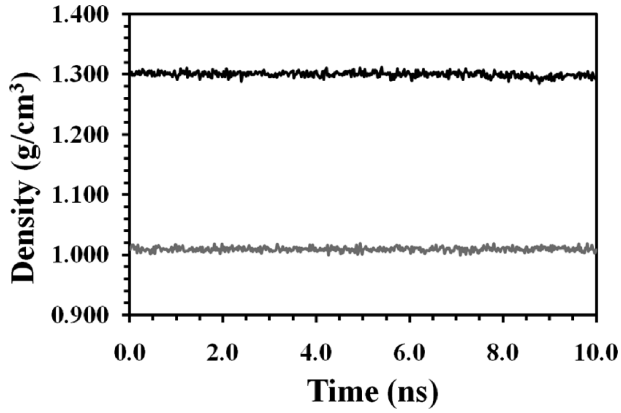

Figure 1. Temporal evolution of the density during the *NPT* (300 K and 1 atm) MD simulations performed on model **I** considering two different force fields: **FF1** (gray) and **FF8** (black).

TABLE 5: Averaged Density (ρ) and Energy (*E*) Obtained for Models II, III, and IV Derived from MD Simulations Using FF8, QM Geometry Optimizations, and QM/MM Single Point Calculations

no.	model **II**	model **III**	model **IV**
ρ (g/cm^3)[a]	1.288 ± 0.021	1.297 ± 0.011	1.292 ± 0.019
E (kcal/mol)−MD[a]	−8511 ± 87	−8486 ± 101	−8457 ± 51
E (kcal/mol·repeating unit)−QM[b]	−179632 ± 6	−179636 ± 5	−179608 ± 8
E (kcal/mol·repeating unit)−QM/MM[c]	−179627 ± 9	−179621 ± 8	179616 ± 11

[a] Average values considering 10 MD simulations (25 ns long each), which differ in the starting microstructure, for each model. [b] Average values derived from geometry optimizations at the B3LYP/6-31G(d) level on 20 molecular systems for each model. [c] Average values derived from QM/MM single point calculations on 20 randomly selected snapshots for each model.

On the Chemical Structure of PAni-EB

NPT-MD simulations were run using the **FF8** force field and considering the 10 microstructures generated for models **II**, **III**, and **IV**. For each trajectory, the simulation conditions were identical to those described in the previous section. Each trajectory was 25 ns long, which represents a total of (3 models × 10 microstructures × 25 ns each) = 750 ns.

Table 5 lists the averaged values of the density and the energy obtained for models **II**, **III**, and **IV**. As can be seen, the experimental density was very well reproduced by the three examined models, being overestimated by only 3.4%, 4.2%, and 3.8% for **II**, **III**, and **IV**, respectively. It should be remarked that the density of PAni-EB is higher than that typically found for heterocyclic conducting polymers; e.g., the density of amorphous undoped polythiophene is 1.01−1.03 g/cm^3.[9] Therefore, to achieve a satisfactory description of the density of PAni-EB is a challenge for simulation methods, results displayed in Table 5 evidencing the suitability of **FF8**.

On the other hand, the averaged energies displayed in Table 5 indicate that model **II** is slightly more favored than models **III** and **IV**, the latter being the least stable system. However, the confidence of this stability order is limited by the standard deviations, which suggest that the three models are within similar energy intervals. In order to get a deeper insight into the stability order, additional calculations on models **II**, **III**, and **IV** have been performed using quantum mechanics (QM) and quantum mechanics/molecular mechanics (QM/MM) methodologies. More specifically, 2 snapshots were randomly selected from each of the 10 MD trajectories run for each of the 3 considered models. After this, for each of the [(2 snapshots) × (10 starting microstructures) × (3 molecular models)] = 60 selected snapshots, a molecular fragment consisiting of a number of repeating units ranging from 6 to 16 was randomly chosen. The only restriction in this choice was that molecular fragments of models **II** and **III** involved the same number of AM and IM repeating units, and the total number of AM units contained in the 20 fragments of model **IV** was identical to that of IM units. After addition of the hydrogen atoms to the phenyl rings transforming the CH pseudoatoms into two explicit atoms and blocking of the ends of all the molecular fragments with hydrogen atoms, geometry optimizations were performed using the B3LYP functional[22] combined with the 6-31G(d) basis set,[23] i.e., the B3LYP/6-31G(d) level. The averaged QM molecular energy for each model (expressed in kcal/mol per repeating unit) is included in Table 5. Models **II** and **III**, in which AM and IM units are arranged alternatively and randomly, respectively, are practically isoenergetic at the molecular level, while model **IV** is unfavored by more than 20 kcal/mol per repeating unit. It should be noted that conformational effects are included in these results since geometry optimizations were performed using starting points different for arrangements produced during the MD simulations. Accordingly, the averaged QM energies clearly indicate that intramolecular AM···IM interactions are favored with respect to intramolecular AM···AM and IM···IM interactions.

QM/MM calculations were performed using the snapshots previously selected for QM geometry optimizations. More specifically, the molecular fragments used as starting points for QM calculations were described at the B3LYP/6-31G(d) level, while all the AM and IM residues with at least one particle within a cutoff distance of 10.0 Å were represented as point charges. The QM/MM method was used for single point calculations, i.e., energy evaluation using the coordinates produced by MD, rather than for geometry optimization. The averaged energies, which are included in Table 5, are fully consistent with both MD and QM results reflecting that models **II** and **IV** are the most and least favored, respectively, even though the differences between **II** and **III** are considerably small. Accordingly, the MD, QM, and QM/MM energies displayed in Table 5 indicate that the chemical structure of PAni-EB should be ideally described as an alternated disposition of AM and IM units and, more realistically, as an alternation of small blocks with a few AM or IM units. Thus, the three methodologies used to evaluate the stability of the different models indicate that AM···IM interactions are the most favored not only at the intermolecular level but also at the intramolecular one.

On the Three-Dimensional Organization of PAni-EB

The three-dimensional organization of the molecular chains in PAni-EB has been examined by using the partial radial

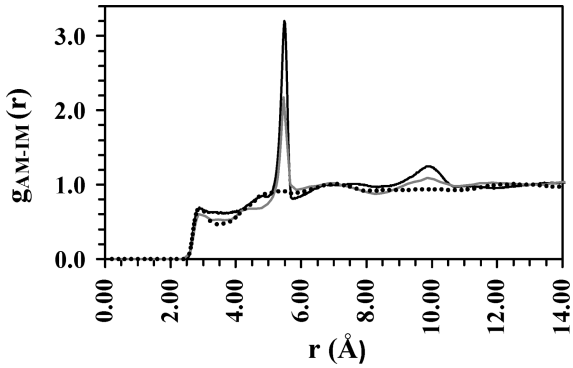

Figure 2. Partial radial distribution function of AM···IM pairs calculated for models **II** (black solid line), **III** (gray solid line), and **IV** (black dotted line).

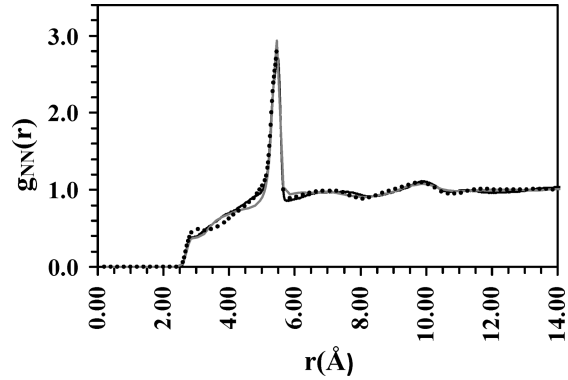

Figure 3. Partial radial distribution function of N···N pairs calculated for models **II** (black solid line), **III** (gray solid line), and **IV** (black dotted line).

distribution functions. Figure 2 displays the partial distribution of the AM···IM pairs, $g_{AM-IM}(r)$, for models **II**, **III**, and **IV**. The radial distribution functions, which represent the probability of finding a pair of repeating units in terms of distance, have been calculated with respect to the center of masses. As it can be seen, the functions obtained for each model present some distinctive features. Model **II** shows a sharp and narrow peak at 5.5 Å, which is due to the adjacent AM−IM units in the chain. This alternated sequence is also responsible for the small and broad peak at 10.0 Å. Similar but less intense peaks are detected for model **III**, in which covalently linked AM and IM units are relatively frequent due to its random chemical structure. However, this peak is absent in model **IV** indicating that AM and IM units are not organized in ordered phases. Indeed, excluding the peaks associated with the chemical sequences, the microstructures obtained for the three models under study do not display three-dimensional order in the organization of AM and IM repeating units. On the other hand, no significant differences among the three models were detected from the partial distributions of the AM···AM and IM···IM pairs (data not shown).

Figure 3 represents the partial distribution functions calculated for the N···N pairs, $g_{NN}(r)$. As can be seen, the profiles are very similar for the three models. Thus, the sharp and narrow peak at 5.5 Å corresponds to the distance between two adjacent repeating units, independent of their AM or IM nature, while the broad and small peak at around 9.9 Å should be attributed to nitrogen atoms of the same chain belonging to repeating units separated by two phenyl rings. In contrast, the small shoulders found for some models at around 3 and 7 Å are consequence of the short-range intermolecular interactions. Similarly, no distinctive structural feature among the different models was

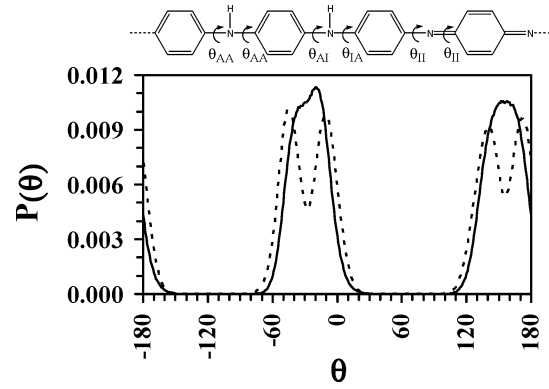

Figure 4. Dihedral angle (in degrees) distribution for PAni-EB chains produced using models **II** and **III**. The dihedral angles involving AM (θ_{AA} and θ_{AI}) and IM (θ_{IA} and θ_{II}) are represented by solid and dashed lines, respectively.

obtained from the distribution functions associated with the CH···CH and CH···N pairs (data not shown).

The flat profiles displayed in Figures 2 and 3, which predict that amorphous PAni-EB only exhibits short-range intramolecular correlation, are fully consistent with the radial distribution function analysis of X-ray scattering data reported by Winokur and co-workers.[24] These authors found that all the well-defined features in the radial distribution function obtained for amorphous PAni-EB samples were due to intrachain pair correlations, while interchain pair correlations only form a smoothly varying background.

Figure 4 shows the torsional angle distribution of the PAni-EB chains obtained for models **II** and **III**, even though very similar results were obtained for model **IV** (data not shown). Dihedral angles have been categorized in two groups. The profile obtained for the first one, which involves the rotation of all the bonds contained in AM units (θ_{AA} and θ_{AI} in the molecular scheme included in Figure 4), shows two broad peaks centered at around −30° and 160°. These are fully consistent with the dihedral angles predicted from quantum mechanical calculations for a system formed by a single molecular chain, i.e., the values of the dihedral angles found for the minimum energy conformations were −17°, −36°, 146°, and 163°.[2f] The second group contains the dihedrals defined by the rotation of bonds involving at least one atom contained in IM units (θ_{IA} and θ_{II} in Figure 4). The distribution shows four sharp peaks with the maxima located at −46°, −11°, 141°, and 167°, which are in very good agreement with the values found for a single molecular chain using quantum mechanical calculations, i.e., −47°, −8°, 139°, and 172°.[2f] These results allow the conclusion that molecular packing interactions do not induce significant changes in the molecular conformation, which is very reasonable taking into account the rigidity imposed by phenyl rings.

The presence of N−H···N hydrogen bonding interactions has been examined for the three considered models. For this purpose, the distance between the N−H groups (hydrogen bonding donors) of the AM units and the N atoms (hydrogen bonding acceptors) of both AM and IM units have been determined. Hydrogen bonds have been considered to exist when the (N−)H···N distance is lower than 2.50 Å. Results, which are expressed as the average percentage of AM units acting as hydrogen bonding donors in both AM···AM and AM···IM interactions, are summarized in Table 6. As can be seen, AM···AM hydrogen bonds are much less frequent than AM···IM interactions, independent of the model. Moreover, the population of AM···AM hydrogen bonds is very similar

TABLE 6: Distribution of AM···AM and AM···IM Hydrogen Bonds Derived from MD Simulations on Models II, III, and IV[a]

no.	AM···AM	AM···IM
model **II**	4.5 ± 1.0	19.4 ± 1.9
model **III**	4.6 ± 1.1	17.2 ± 2.4
model **IV**	5.4 ± 1.4	15.6 ± 1.7

[a] The distributions are expressed as percentage (on average) of AM units acting as hydrogen bonding donor in AM···AM and AM···IM interactions. Standard deviations are also displayed.

for all three models (ranging from 4.5% to 5.4%). However, model **II** shows a slightly clear tendency to have a larger number of AM···IM hydrogen bonds (19.4%) than model **IV** (15.6%). This result indicates that the alternated arrangement of AM and IM units in model **II** compared to the segregated distribution of AM and IM units in model **IV** favors the formation of hydrogen bonds, explaining the lower energy of the former model (Table 5). These results are fully consistent with the FTIR experiments early reported by Zheng et al., which evidenced that the AM···IM hydrogen bonds are favored with respect to AM···AM ones.[4a] These authors concluded that intermolecular hydrogen bonds between imine and amine nitrogen sites are predominately responsible for the aggregate formation in "as-synthetized" PAni-EB powder. Thus, although it was not possible to determine the frequency of these interactions nor the number of interchain hydrogen bonds that are necessary to form aggregate, a "zipper effect" was proposed whereby additional AM···AM and AM···IM hydrogen bonds and possibly other types of interactions might proceed between chains already joined by at least one AM···IM hydrogen bond.[4a]

Conclusions

In this work we present a comprehensive theoretical study about the microscopic structure of amorphous PAni-EB. For this purpose, 0.8 μs of *NPT*-MD, distributed in 38 different trajectories, have been run considering molecular models made of four polymer chains packed within a simulation box. Moreover, QM and QM/MM calculations have been performed to support some of the reached conclusions.

Analysis of different force fields evidenced that simulation of this polycyclic system using classical MD is not an easy task, which should be mainly attributed to its high density. Thus, the experimental density was significantly underestimated by many of the force fields tested in this work. We found that the van der Waals parameters reported for C and H in GROMOS[13] and MM2[15] force field are not able to describe the characteristics of the phenyl rings of PAni-EB. However, an excellent description of the density was derived from the following combination, which has been denoted **FF8**: (i) electrostatic charges derived from quantum mechanical calculations at the HF/6-31G(d) level; (ii) van der Waals parameters extrapolated from the GROMOS 53A6 force field for all the atoms with exception of the C−H of the phenyl rings; and (iii) the van der Waals parameters for the CH pseudoatoms developed by MacKie and co-workers[18] to describe the properties of liquid benzene.

Analysis of the energies obtained by MD as well as those derived from additional QM and QM/MM calculations indicates that models **II** and **III** are more stable than model **IV**. This is due to the AM···IM interactions, which are the most favored at both intramolecular and intermolecular levels. The chemical structure of PAni-EB has been conceived as an alternation of very short blocks of AM and IM units, which can be idealized as an alternated disposition of AM and IM. On the other hand, the calculated partial radial distribution functions reflect that amorphous PAni-EB only shows short-range intramolecular pair correlation. The absence of intermolecular order is fully consistent with available experimental data.[24] In spite of such disorder, the population of AM···IM hydrogen bonds has been found to be significantly higher than that of AM···AM ones, which is also consistent with FTIR results.[4a] The distribution of dihedral angles derived from MD simulations is in excellent agreement with the values found from QM calculation on systems formed by a single molecular chain,[2f] indicating that the effect of the intermolecular interactions on the conformation is very small.

Acknowledgment. Gratitude is expressed to the Centre de Supercomputació de Catalunya (CESCA). Financial support from the MICINN and FEDER (MAT2009-09138 and FIS2009-13641-C02-01) and Generalitat de Catalunya (research groups 2009 SGR 925, 2009 56R 1003, and XRQTC) is gratefully acknowledged. Support for the research of C.A. was received through the prize "ICREA Academia" for excellence in research funded by the Generalitat de Catalunya.

References and Notes

(1) (a) Brédas, J. L. *Adv. Mater.* **1995**, *7*, 263. (b) Brédas, J. L.; Cornil, J.; Beljonne, D.; Dos Santos, D. A.; Shuai, Z. *Acc. Chem. Res.* **1999**, *32*, 267. (c) Casanovas, J.; Alemán, C. *J. Phys. Chem. C* **2007**, *111*, 4823. (d) Zade, S. S.; Bendikov, M. *Org. Lett.* **2006**, *8*, 5243. (e) Hutchison, G. R.; Ratner, M. A.; Marks, T. J. *J. Am. Chem. Soc.* **2005**, *127*, 2339. (f) Casanovas, J.; Zanuy, D.; Alemán, C. *Polymer* **2005**, *46*, 9452. (g) Tian, Y.-H.; Park, G.; Kertesz, M. *Chem. Mater.* **2008**, *20*, 3266. (h) Torras, J.; Bertran, O.; Alemán, C. *J. Phys. Chem. B* **2009**, *113*, 15196. (i) Rodríguez-Ropero, F.; Zanuy, D.; Alemán, C. *Polymer* **2010**, *51*, 308.

(2) (a) Kwon, O.; McKee, M. L. *J. Phys. Chem. B* **2000**, *104*, 1686. (b) Cavazzoni, C.; Colle, R.; Farchioni, R.; Grosso, G. *Phys. Rev. B* **2002**, *66*, 165110. (c) Zhekova, H.; Tadjer, A.; Ivanova, A.; Petrova, J.; Gospodinova, N. *Int. J. Quantum Chem.* **2007**, *107*, 1688. (d) Lim, S. L.; Tan, K. L.; Kang, E. T.; Chin, W. S. *J. Chem. Phys.* **2000**, *112*, 10648. (e) Varela-Álvarez, A.; Sordo, J. A.; Scuseria, G. E. *J. Am. Chem. Soc.* **2005**, *127*, 11318. (f) Alemán, C.; Ferreira, C. A.; Torras, J.; Meneguzzi, A.; Canales, M.; Rodrigues, M. A. S.; Casanovas, J. *Polymer* **2008**, *49*, 5169. (g) Casanovas, J.; Canales, M.; Ferreira, C. A.; Alemán, C. *J. Phys. Chem. A* **2009**, *113*, 8795.

(3) Angelopoulos, M.; Asturias, G. E.; Ermer, S. P.; Ray, A.; Scherr, E. M.; MacDiarmid, A. G.; Akhtar, M.; Kiss, Z.; Epstein, A. J. *Mol. Cryst. Liq. Cryst.* **1988**, *160*, 151.

(4) (a) Zheng, W.; Angelopoulos, M.; Epstein, A. J.; MacDiarmid, A. G. *Macromolecules* **1997**, *30*, 2953. (b) Yang, D.; Zuccarello, G.; Mattes, B. R. *Macromolecules* **2002**, *35*, 5304.

(5) Avlyanov, J. K.; Min, Y.; MacDiarmid, A. G.; Epstein, A. J. *Synth. Met.* **1995**, *72*, 65.

(6) Lee, C. K.; Hua, C. C.; Chen, S. A. *J. Phys. Chem. B* **2009**, *113*, 15937.

(7) (a) Ostwal, M. M.; Tsotsis, T. T.; Sahimi, M. *J. Chem. Phys.* **2007**, *126*, 124903. (b) Ostwal, M. M.; Sahimi, M.; Tsotsis, T. T. *Phys. Rev. E* **2009**, *79*, 061801.

(8) Bhadra, S.; Khastgir, D. *Synth. Met.* **2009**, *159*, 1141.

(9) Curcó, D.; Alemán, C. *J. Comput. Chem.* **2007**, *28*, 1743.

(10) Curcó, D.; Alemán, C. *J. Chem. Phys.* **2003**, *119*, 2915.

(11) Curcó, D.; Laso, M.; Alemán, C. *J. Phys. Chem. B* **2004**, *108*, 20331.

(12) Stejskal, J.; Gilbert, R. G. *Pure Appl. Chem.* **2002**, *74*, 857.

(13) Oostenbrink, C.; Villa, A.; Mark, A. E.; van Gunsteren, W. F. *J. Comput. Chem.* **2004**, *25*, 1656.

(14) Hariharan, P. C.; Pople, J. A. *Chem. Phys. Lett.* **1972**, *16*, 217.

(15) (a) Allinger, N. L. *J. Am. Chem. Soc.* **1977**, *99*, 8127. (b) Profeta, S.; Allinger, N. L. *J. Am. Chem. Soc.* **1985**, *107*, 1907.

(16) Wick, C. D.; Martin, M. G.; Siepmann, J. I. *J. Phys. Chem. B* **2000**, *104*, 8008.

(17) Errington, J. R.; Panagiotopoulos, A. Z. *J. Chem. Phys.* **1999**, *111*, 9731.

(18) Contreras-Camacho, R. O.; Ungerer, P.; Boutin, A.; Mackie, A. D. *J. Phys. Chem. B* **2004**, *108*, 14109.

(19) (a) Berendsen, H. J. C.; van der Spoel, D.; van Drunen, R. *Comput. Phys. Commun.* **1995**, *91*, 43. (b) Lindahl, E.; Hess, B.; van der Spoel, D.

J. Mol. Model. **2001**, *7*, 306. (c) Van Der Spoel, D.; Lindahl, E.; Hess, B.; Groenhof, G.; Mark, A. E.; Berendsen, H. J. C. *J. Comput. Chem.* **2005**, *26*, 1701–1718. (d) Hess, B.; Kutzner, C.; van der Spoel, D.; Lindahl, E. *J. Chem. Theory Comput.* **2008**, *4*, 435.

(20) Darden, T.; York, D.; Pedersen, L. *J. Chem. Phys.* **1993**, *98*, 10089.

(21) Berendsen, H. J. C.; Postma, J. P. M.; van Gunsteren, W. F.; DiNola, A.; Haak, J. R. *J. Chem. Phys.* **1984**, *81*, 3684.

(22) (a) Becke, A. D. *J. Chem. Phys.* **1993**, *98*, 1372. (b) Lee, C.; Yang, W.; Parr, R. G. *Phys. Rev. B* **1988**, *37*, 785.

(23) Hariharan, P. C.; Pople, J. A. *Theor. Chim. Acta* **1973**, *28*, 213.

(24) Maron, J.; Winokur, M. J.; Mattes, B. R. *Macromolecules* **1995**, *28*, 4475.

JP1052584